Numerical Simulation of Sub-cooled Boiling Flow with Fouling Deposited Inside Channels

X. Liu[a,c*], X. Zhang[b], T. Lu[a], K. Mahkamov[c], H. Wu[c], M. Mirzaeian[d]**

[a]Faculty of Material and Energy, Guangdong University of Technology, Guangzhou, 510006, China
[b]Sino-French Institute of Nuclear Engineering and Technology, Sun-Yat-Sen University, Zhuhai,519082,China
[c]Department of Mechanical and Construction Engineering, Faculty of Engineering and Environment, Northumbria University, Newcastle upon Tyne, NE1 8ST, United Kingdom
[d]School of Engineering and Computing, University of the West of Scotland, PA1 2BE. United Kingdom
*Corresponding author: X. Liu, Email: forlxy@163.com; Tel. +44(0) 751 8297081
**Corresponding author: H. Wu, Email: hongwei.wu@northumbria.ac.uk; Tel. +44(0) 191 349 5365

Abstract: In this article, a numerical simulation has been performed to investigate the sub-cooled boiling flow in axisymmetric channels using the two-phase particle model. The equivalent diameter of the channel is 4.38 mm with 365.7 cm in length. The fouling deposited layer is filled with subsequent two-thirds of the flow channel. The internal surface of the channel is covered by a fouling deposit layer with a thickness ranging from 0.225 mm to 1.55 mm. Uniform heat flux of 29267.6 W/m^2 is applied on the heated wall. Validation of the CFD model is carried out through comparison with open published experimental data and a close agreement is achieved. A new parameter, Security factor, is introduced and defined in the current study. Numerical results show that the developed two-phase particle model could well predict the water-steam two-phase change flow. The Nusselt number in the fouling region without fouling deposited could be 50 times higher than that with fouling layer. The heat transfer performance of the channel with thickness of 0.225 mm fouling deposit layer is 5 times larger than that with thickness of 1.55 mm fouling deposit layer. It is also found that the inlet velocity has significant impact on the boiling and total pressure drops along the channel.

Keywords: sub-cooled, numerical simulation, boiling, fouling, heat transfer

NOMENCLATURE

A_w	whole surface is covered with bubbles of the wall (m^2)	M_a	momentum from phase β to phase a (kg·m/s)
C_P	specific heat capacity (J/kg·K)	$m_{a\beta}$	transfer of mass from phase β to phase a (kg/s)
d_w	bubble detachment diameter (mm)	Z	distance along the channel (m)
E_a	energy from phase β to phase a (W)	***Greek letters***	
L	length of the channel (m)	h	heat transfer coefficient (W/m^2·K)

h_a	enthalpy of phase *a* (J/kg)	r	volume fraction (-)
Nu	Nusselt number (-)	μ	effective viscosity (Pa·s)
P_a	pressure of phase *a* (Pa)	λ	thermal conductivity (W/m·K)
q_w	wall heat flux (W/m^2)	ρ	density (kg/m^3)
SF	security factor	***Subscripts***	
T_a	temperature of phase *a* (K)	α	Phase
T_w	wall temperature (K)	β	Phase
T_{sat}	saturation temperature *(K)*	w	Wall
U_a	velocity of phase *a* (m/s)	m	Average

1. INTRODUCTION

Development of two phase channel technology requires a comprehensive fundamental understanding of virtually all hydrodynamic and thermal aspects of phase change in small channels. Thus, the ability to accurately predict flow boiling heat transfer for a given channel geometry under different operating conditions is of paramount important to the performance assessment of a small channels, especially with fouling deposit layer inside the channels. Many studies have been devoted to the heat transfer performance of the flow boiling in small channels over the past decades. Various available correlations of the saturated flow boiling heat transfer of the vertical tubes were summarized in a systematic manner [1-3]. Kandikar [4] developed a new flow boiling map to depict the relationships among the heat transfer coefficient, quality, heat flux, and mass flux for different fluids in the subcooled and the saturated flow boiling regions. It was found that the trends observed in the experimental data and correlations for water and refrigerants could be used in deriving the flow boiling map. Gupta et al. [5] carried out an experimental investigation to determine the local forced convective boiling heat transfer coefficient in small tube bundles consisting of horizontal tubes in a vertical column arranged in a large channel under low cross-flow velocities in saturated distilled water at atmospheric pressure. A Chen-type relation has been used to correlate the data

on local forced convective heat transfer coefficients of upper tubes with reasonably accuracy. Kumar et al. [6] conducted an experimental study to measure the enhancement in the nucleate pool boiling heat transfer of upper heating tubes of copper. A model was developed to predict the heat transfer coefficient of individual tube in a multi-tube row and the bundle heat transfer coefficient. Da Silva et al. [7] presented an experimental investigation of nucleate boiling on a vertical array of horizontal plain tubes. A general correlation for the prediction of the nucleate boiling heat transfer coefficient on a vertical array of horizontal tubes under flooded conditions was proposed. The new correlation compared reasonably well with independent data from the literature. Mishima and Hibiki [8] performed an experimental study for air-water two-phase flow in capillary tubes to measure flow regime, void fraction, rising velocity of slug bubbles and frictional pressure loss. The void fraction was correlated well by the drift flux model with a new equation for the distribution parameter as a function of inner diameter. The rise velocity of the slug bubbles was also correlated well by the drift flux equation. Lee and Lee [9] proposed new correlations for the two-phase pressure drop through horizontal rectangular channels with small gaps at atmospheric pressure. The two-phase frictional multiplier was expressed using the modified Lockhart-Martinelli type correlation. Shannak [10] conducted an experimental investigation of the air water two-phase flow frictional pressure drop of vertical and horizontal smooth and relatively rough pipes, respectively. A new prediction model for frictional pressure drop of two-phase flow in pipes was proposed and the proposed model fits the experimental data very well for vertical, horizontal, smooth and rough pipes. Chen et al. [11] carried out an experimental study to measure the frictional pressure drops for water single-phase and two-phase air-water flow in three small rectangular channels. A modified C factor of Chisholm method considering the effect of aspect ratio was proposed and this correlation was valid in wide ranges of mass flux, gas quality, Martinelli

parameter and aspect ratio.

On the numerical side, many researchers used computational fluid dynamic (CFD) simulation to estimate the hydrodynamics of two phase flow. Tryggvason et al. [12] applied the Eulerian multiphase flow model to investigate the boiling process in a coiled tube. It was found that the phase distributions showed a continuous stratification in the horizontal tubes and were influenced by both buoyancy force and centrifugal force in the tube bends. Simulation of flow boiling in vertical pipes using CFX-5 CFD codes showed good agreement with experimental results [13]. Boiling at walls was also modeled with a wall heat flux partitioning model and the turbulence induced by the bubbles also was taken into account in turbulence modeling. Yang et al. [14] presented a numerical simulation, using the VOF multiphase flow model, and the corresponding experiments to investigate the boiling flow of R141B in a horizontal coiled tube. Their numerical predictions of phase evolution were in a good agreement with the experimental observations, and the two phase flow in the tube bends was much more complicated due to the influence of liquid-vapor interaction with the interface evolution. Yuan et al. [15] performed numerical simulation on the natural convection film boiling and forced convection film boiling on a sphere at saturated conditions. Their results showed that numerical simulations with the interface tracking method to study the transient and dynamic aspects of liquid-vapour phase change could be a promising prospect. Mazumder [16] performed CFD analysis of single- phase and two-phase flow in a 90 degree horizontal to vertical elbow with 12.7 mm inside diameter. Characteristic flow behaviour was investigated at six different upstream and downstream locations of the elbow. Comparison of CFD results with available empirical models showed reasonably good agreement. Giannoulis and Margaris [17] numerically studied a two-phase buoyancy driven flow within a 20 m of the riser tube. The numerical solution of the discretized two-dimensional Navier-Stokes equations over a structured grid with quadrilateral elements was accomplished with

FLUENT package. Saffari et al. [18] simulated the effects of the pipe diameter, coil diameter, and coil pitch on the single-phase and two-phase (air-water) bubbly fluid flows. It was concluded that the friction coefficient increases with an increase in the curvature, pipe diameter and coil pitch, whereas decreases with an increase in the coil diameter and void fraction. Harikrishnan et al. [19] implemented a new solver called Boiling-Foam to simulate the sub-cooled boiling flow in vertical pipes. It was found that the solver can predict the parameters correctly in some regions which are very close to the heated wall. As for the fouling studies, Changani et al. [20] and Youcef et al. [21] carried out the study on the fouling of processing heat exchangers used for heating dairy fluids such as pasteurizing and sterilizing milk in dairy industry. Their results showed that the aggregation rate of unfolded protein was found to increase exponentially with increasing wall temperature, and the rate of cleaning depends on both the deposit present and the type of chemical treatment used. Some researchers have studied the deposition process in fouling in the steam generators of pressurized water reactors, and found multiple factors affect to deposit formation rate [22]. The material used for the heat-transfer pipes and the physicochemical properties of the metal used in the components of the second-loop equipment of a nuclear power plant also affect deposit of fouling [23]. The formed deposits and sludge can be removed from the heat exchangers by chemical and mechanical means , and combinations of chemical and mechanical cleaning can be superior to mechanical cleaning alone for certain combinations of parameters [24]. Sepehr Sanaye[25] used the optimization algorithm to optimize the fouling cleaning schedule in a heat exchanger network. S. Jun , V.M. Puri[26] carried out 2D simulation in milk pasteurizer process , the predicted mass deposit values at each channel were in good agreement with the experimental data, and results can be used to determine the sensor locations that can provide needed information on the degree of fouling to monitor and cleaning process . Mariusz Markowski, et al[27] presented a novel method for on-line determination of the thermal resistance of fouling in shell and tube

heat exchangers by considering parameters such as splitting operation period and consecutive time intervals etc. M.S. Abd-Elhady et al[28] carried out fouling experiments with particles of different sizes and different materials running under different gas speeds. It is found that the smallest particles in the flow deposit on the tubes of the heat exchanger at areas of minimum flow velocities, and then the large particles deposit and the fouling layer starts to build up, and there is a critical flow velocity to prevent fouling deposited and the gas speed of a HE should be larger than the critical flow velocity. Mariusz Markowski[29] studied the influence of fouling on heat exchanger with a decision making model of optimal cleaning schedule correspond to the maximum of avoided economic loss. Results show that the cleaning interventions scheduled saved about 5% of the maximum attainable value of energy. Mostafa et al. [30] studied the effect of the surface temperature on the fouling rate. The setup was constructed using a test tube with 3 m in length and 5.53 cm in inner diameter, and three different electric heaters fixed at the center. Results showed that the asymptotic fouling resistance decreased as the surface temperature increased under the same operating conditions, especially in the surface temperature range from 55 °C to 71°C.The objective of the present study is to examine the wall temperature at different fouling deposit layers on the sub-cooled water flow inside channel under a uniform heat flux along the heated wall. In the current work, the equivalent diameter of the channel is 4.38 mm with a 365.7 cm in length. Water is selected as the working fluid and it enters the channel as liquid and the outlet pressure is 0.438 MPa. The heat capacity of fouling layer and the heated wall are not uniform along the channel. The arrangement of channel is finned.

2. Geometrical configurations

Published experimental data showed that there would be high shear acting on wall films inside the long channel. The reason could be that the flow would be largely shear dominated and followed by the

gravitational effects. Since the test model is axial symmetry, the computational domain can be simplified to a quarter in tube channel of two-phase flow with three solid domains and one fluid domain. Figure 1 demonstrates the geometrical model and the mesh generated in the present work. The three solid domains are (i) alloy steel tube, (ii) aluminium fin, and (iii) fouling layer, respectively. There is only one fluid domain which is water-vapour two-phase flow. The fouling layer occurs at two thirds of the total length from the inlet. Table 1 lists the detailed geometrical parameters of the model. Figure 2 shows the sketch of the fins. In the current work, there are six wide fins and three thin fins along the channel and these fins can significantly influence the fluid flow.

It is well recognized that the thermal conductivity and heat capacity of the steel tubes (the heated wall) varies with the bulk temperature, and they were determined by experiment. The thermal conductivity and heat capacity of the steel tubes can be correlated using the available experimental data as follows:

$$k = 3.46\times10^{-6}T^2 + 0.00173T + 13.45 \ [W/m^2\cdot K] \quad (1)$$

$$C_P = 8.65\times10^{-6}T^2 + 3.46\times10^{-5}T + 0.1142 \ [J/kg\cdot K] \quad (2)$$

where, the T is Kelvin temperature of the heated wall.

The cross section of the geometrical model is presented in Figure 3. The symbol of s in Figure 3 denotes the thickness of the deposited fouling layer. The thicknesses of the fouling layer are 0, 0.225, 0.45, 0.675, 0.9 and 1.55 mm, respectively. The gap between the heated wall and the aluminium fin is 1.55 mm, and it is easy to understand that the fouling can fill the gap with the deposited fouling thickness of 1.55 mm where the two-third region between the steel tube and the aluminium fins will be fully filled with deposited fouling layer.

3.1. Governing equations

In the present study, steady-state solvers for buoyant, turbulent flow of the incompressible fluids will be taken into account. The continuous phase is liquid and the dispersed phase is gaseous.

Continuity equation:

$$\nabla\cdot(\rho_\alpha r_\alpha U_\alpha) = \dot{m}_{\alpha\beta} - \dot{m}_{\beta\alpha} \tag{3}$$

Momentum equation:

The momentum equation for each phase is solved separately. The momentum equation for phase *a* is given as:

$$\nabla\cdot[r_\alpha\{\rho_\alpha U_\alpha \otimes U_\alpha - \mu_\alpha(\nabla U_\alpha + (\nabla U_\alpha)^T)\}] = M_\alpha - r_\alpha \nabla P_\alpha + r_\alpha \rho_\alpha g + (\dot{m}_{\alpha\beta} U_\beta - \dot{m}_{\beta\alpha} U_\alpha) \tag{4}$$

and the energy equation for phase *a* follows as:

Energy equation:

$$\nabla\cdot(r_\alpha(\rho_\alpha U_\alpha h_\alpha - \lambda_\alpha \nabla T_\alpha)) = \dot{m}_{\alpha\beta} h_\beta - \dot{m}_{\beta\alpha} h_\alpha + Q_\alpha + E_\alpha \tag{5}$$

Due to the lower density of vapor, it is commonly assumed that, in sub-cooled boiling flow, the motion of the dispersed vapor phase follows the fluctuations in the continuous liquid phase; therefore, the turbulent stresses are modeled only for the liquid phase. A $k-\varepsilon$ turbulence model is employed for the continuous phase while the dispersed vapor phase remains laminar.

3.2. Modeling of boiling

Boiling models are used to compute the rate of the bubble formation and evaporation at the heated walls.

Wall heat flux partitioning:

The wall boiling phenomena is modelled with the heat flux partitioning model [33]). Accordingly, the heat flux applied to the external wall is written as a sum of the three heat fluxes as:

$$Q_{total} = Q_{conv} + Q_{quench} \tag{6}$$

Q_{conv}, Q_{quen}, *and* Q_{evap}, represent the convective, quenching and evaporative heat fluxes, respectively. They are modelled as a function of the wall temperature and local flow parameters. Eq. (6) is solved iteratively for the local wall temperature, T_w, which satisfies the wall heat flux partitioning. Each of the heat flux component can be modelled as given below.

The turbulent convection is modelled exactly as that of turbulent single phase convection as:

$$Q_{conv} = h_c(1-A_w)(T_w - T_l) \tag{7}$$

where, h_c is the convection heat transfer coefficient that is calculated as:

$$h_c = S_t \rho_l c_{pl} u_l \tag{8}$$

where S_t is the Stanton Number, $S_t = Nu/RePr$, u_l is the velocity of the first control volume which parallel to the heated wall, and the subscript *l* represents the liquid phase.

The quenching heat flux is modelled by:

$$Q_{quen} = h_Q A_w (T_w - T_l) \tag{9}$$

$$h_Q = \frac{2}{\sqrt{\pi}} f \sqrt{t_{wait} \lambda_l \rho_l C_{pl}} \tag{10}$$

f is the bubble detachment frequency and t_{wait} is the waiting time between successive bubble detachments, calculated by $t_{wait} = \frac{0.8}{f}$.

The evaporative heat flux is modelled as:

$$Q_{evap} = \frac{\pi}{6} d_w^3 \rho_g f N'' h_{fg} \tag{11}$$

N'' is the nucleation site density, d_w is the bubble detachment diameter and h_{fg} is the latent heat of vaporization. Nucleation site density is given by:

$$N'' = 0.8 \times 10^6 \left(\frac{T_w - T_l}{\Delta T_{reff}}\right)^{1.805} \tag{12}$$

Bubble detachment frequency is modelled as:

$$f = \sqrt{\frac{4g(\rho_l - \rho_g)}{3C_D d_w \rho_l}} \tag{13}$$

Due to its dependence on gravity, this correlation is taken from pool boiling. It is simply estimated as the bubble rise velocity divided by the bubble departure diameter. The drag coefficient factor C_D is calculated by:

$$C_D = \frac{24}{\mathrm{Re}}(1 + 0.1\mathrm{Re}^{0.75}) \tag{14}$$

Bubble detachment diameter depends upon many control factors, i.e., heat flux, system pressure, liquid properties. The diameter can be modelled as:

$$d_w = d_{ref} e^{\frac{T_{sat} - T_l}{\Delta T_{reff}}} \tag{15}$$

where d_{ref} is taken as 0.6 mm, and ΔT_{ref} = 45 K.

The wall area fraction influenced by the vapour bubble is calculated by:

$$A_w = \pi(a\frac{d_w}{2})^2 N'' \tag{16}$$

where, a is the bubble influence factor. A_w=1 indicates that the whole surface is covered with bubbles.

The heat transfer coefficient along the axial length of the model, α, is then calculated from the heat flux, outside wall temperature and local saturation temperature deduced from the local pressure.

$$\alpha = \frac{\mathrm{q}_w}{T_w - T_{sat}(p)} \tag{17}$$

To evaluate the effect of the two phase heat transfer inside the channel, Nusselt number is defined as follows：

$$Nu = \frac{\alpha L}{\lambda_m} \tag{18}$$

where, $h = \frac{q_w}{\alpha_w - \alpha_{sat}}$, and $\lambda_m = \gamma_\alpha \lambda_\alpha + \gamma_\beta \lambda_\beta$

To estimate the safety of the operation system, security factor is defined as follows:

$$SF = \frac{T_w}{T_{saf}} \tag{19}$$

where, T_{safe} is the safety temperature of the tube and it is considered as 700 K for the system in nuclear station; and it is considered that the SF=0.85 is the critical value for the system.

3.3 Boundary conditions

The inlet velocity of the water is 0.0176 m/s, the inlet water temperature is 120 °C, the volume fraction of water is 1, and the volume fraction of vapour is 0. 0. The outlet pressure is 438729.2 Pa. The heat flux for the inner wall of steel tube is 29267.6 W/m^2. Other walls are symmetric except the interface walls. The thermal conductivity of the fouling layer is 0.173 W/m^2·K.

3.4 Mesh Independence

A mesh independence study was conducted to identify an appropriate mesh density for the aimed calculations. Five meshes were investigated ranging from 0.72 million to 1.62 million cells. The mesh designation and number of cells are shown in Table 2. For the purpose of comparison, average bulk temperatures were calculated on the centreline of the outer steel tube for the five different meshes. It can be seen in Figure 4 that the bulk temperature shows typical converging behavior, and the temperature profiles appear to converge to a central solution profile as the mesh density is increased. Analysis of the bulk temperature shows that all simulated structures appear to be similarly modeled even at the lowest mesh resolution. The temperature magnitudes of these structures are also consistent. In the current work, the 1,232,000 cell mesh (M4) was selected for the calculation.

3. Model validation

In the current study, two groups of experimental data from open published literatures were used to

validate the developed model. The experimental data in reference [31] for the case of 250-3 have been used to examine the effect of various parameters and models on the numerical prediction in detail. Figure 5 compares the measured and calculated values of the heat transfer coefficient on equilibrium quality using models examined in the current study. Figure 6 shows another validation of the model used in present study with experimental result given in reference [32] (provided by the original author). It can be seen clearly that the maximum deviation between the experimental data and numerical results was found to be within 10.2%.

4. Results and discussion

After verifying the reliability of the computational model, the influence of the different thicknesses of the fouling layer on two-phase flow inside the channel was investigated. Figure 7(a) shows the effect of the fouling layer thickness on the bulk temperature of the steel wall, whereas Figure 7(b) presents the bulk temperature in the fouling region. It can be seen clearly that the bulk temperature increases with the increase of the fouling layer thickness. It is also noted that there is about 200 K temperature difference between the fouling layer thickness of 1.55 mm and 0 mm. When the thickness is less than 0.9 mm, the bulk temperature increases 30 K for every 0.225 mm thickness, but there is about 70 K temperature difference between the cases with 1.55 mm and 0.9 mm thickness of fouling layer. This can be explained by the fact that when the thickness is 1.55 mm, the deposited fouling layer fills the gap between the tube and the fins in the fouling region; the cross section area of the fluid becomes smaller which results in a significant increase in the heat transfer resistance of the wall. These results show that the fouling thickness can be estimated from the bulk temperature which can be very helpful in making economic plan for cleaning the fouling layer in practical operations. Figure 8 shows the distribution of the total pressure of the two-phase flow inside

the channel with different fouling layers. Since there are 9 fins along the channel, as shown in Figure 1, especially for the flow after 1978.2 m, the distance between the fins are very close, and the Figures 8 has the staircase-like pressure distribution. It can also be seen clearly that the total pressure does not decrease with the increase of the fouling layer thickness along the channel. The distribution of the vapor volume fraction is shown in Figure 9. The onset of the steam is at the location of 0.5 m, and the variation of the volume fraction changes irregular for all the channels. This may be induced due to a combination of different impact factors, since the boiling within the channel is determined by multiple factors such as the rate of the bubble formation, bubble detachment frequency, waiting time and other factors as described above in the model of the wall boiling. Figure 10 represents the steam volume fraction contours at seven different cross sections along the channel with the fouling thickness of 1.55 mm. The seven cross sections are labeled in Figure 2. It can be seen that the cross section of the fluid for E, F and G become smaller and the steam volume fraction contours are not symmetrical. Besides, the maximum volume fraction of the vapor is lower than 1.0. Figure 11 presents the water (liquid) temperature along the channel at different fouling layer thicknesses. It is noted that the evaporation temperatures are slightly different because different total pressures lead to different evaporation temperature. Figure 12(a) shows the wall Nusselt number along the channel at different fouling thickness. It can be seen that the heat transfer decreases greatly with the presence of the fouling layer, and the Nusselt number drops dramatically with the increase of the fouling thickness compared with that without fouling layer. However, the wall heat transfer effect in the region without fouling shows similar tendency. The mean Nusselt number in the fouling region with deposited fouling layer decreases about 50 times than that without. Figure 12(b) shows that the heat transfer performance with thickness of 0.225 mm is 5 times than the one with thickness of 1.55 mm. The security factor of the

system can be well predicted from Figure 12(c). The system becomes more dangerous with the increase of the fouling thickness, and it shows the system become dangerous with fouling thickness of 1.55 mm.

It is recognized that the inlet velocity could affect both the thermal and hydraulic performance of the two-phase flow inside the channel. Numerical analysis were carried out by varying the inlet velocity (V_{in}) in range of 2-6 times than the original inlet velocity (0.0176 m/s) with the fouling thickness of 1.55 mm. Figure13 shows the bulk temperature distributions along the channel at different inlet velocities. It can be seen that the inlet velocity affect the bulk temperature near the inlet area and near the fins area in the fouling region. However, the pressure drop is higher because of the increased inlet velocity. Figure 14 shows that by increasing inlet velocity 6 times than its original value the pressure drop increases by 57% compared to the pressure drop for the case of original inlet velocity. Figure 15 shows the variation of the vapor volume fraction along the channel at different inlet velocities. The onset of the boiling is delayed with the increase of the inlet velocity, but the maximum volume fractions are similar. Figure 16 presents the variation of the Nusselt number along the channel at different inlet velocities. The relationship between inlet velocity and Nusselt number is not linear, and the effect of inlet velocity on the heat transfer is similar in the fouling region.

5. Conclusions

Numerical simulations have been preformed for three dimensional conjugated heat transfer during water (liquid-vapor) two-phase flow to study the effects of deposited fouling layers on thermal and hydraulic performance. The numerical results are in a good agreement with the available experimental results. Different fouling layer thicknesses are selected to investigate the effect of the deposited fouling on the distributions of the bulk temperature, two-phase flow total pressure, and

water vapor volume fraction and wall heat transfer coefficient.

Results show that for fouling thickness less than 0.9 mm, bulk temperature will increase 30 K for every 0.225 mm thickness, but there are about 70 K temperature difference between the thickness of 1.55 mm and 0.9 mm. The Nusselt number decreases dramatically in the region where the deposited fouling layer forms compared to that without the fouling layer, and the heat transfer effect shows similar tendency for the case of without fouling. The mean Nusselt number in the fouling region with deposited fouling layer decreases about 50 times than that without the fouling layer, and the heat transfer performance with thickness of 0.225 mm is 5 times than that with thickness of 1.55 mm. The system becomes more dangerous with increase of the fouling thickness. Results also show that the inlet velocity affects the onset of boiling and pressure drops and has little impact on the bulk temperature and heat transfer performance in the fouling region.

ACKNOWLEDGMENTS

The authors gratefully acknowledge the financial support from nuclear power plant in China and UK Royal Society (Grant No. RG130646).

REFERENCES:

[1]. Kolev, N. I.. How accurately can we predict nucleate boiling? Thermal and Fluid Science 10(1995)370 – 378.

[2]. Pioro, I. L., Rohsenow, W., and Doerffer, S. S.. Nucleate pool-boiling heat transfer.I: Review of parametric effects of boiling surface, J.International Journal of Heat and Mass Transfer 47(2004) 5033 – 5044.

[3]. Steiner, D., J. Taborek,. Flow boiling heat transfer vertical tubes correlated by an asymptotic model , J. International Journal of Heat Transfer Engineering 13(1992) 43-69.

[4]. Kandlikar, S.G., Development of flow boiling map for subcooled and Saturated Flow Boiling of Different Fluids inside Circular Tubes, ASME Journal of Heat Transfer 113(1991) 190-200.

[5]. Akhilesh Gupta, J.S. Saini, H.K. Varma, Boiling heat transfer in small horizontal tube bundles at low cross-flow velocities. Int. Heat Mass Transfer, 38(1995) 599–605.

[6]. Kumar S., Mohanty B., Gupta S.C.: Boiling heat transfer from vertical row of horizontal tubes. Int. J. Heat Mass Transfer ,45(2002) 3857–3864.

[7]. Robert Pastuszko, Boiling heat transfer enhancement in subsurface horizontal and vertical tunnels, Experimental Thermal and Fluid Science, 32(2008)1564-1577.

[8]. Mishima, L., Hibiki, T., Some characteristics of air–water two-phase flow in small

diameter vertical tubes. International Journal of Multiphase Flow, 22(1996) 703–7l2.

[9]. Han Ju Lee, Sang Yong Lee, Pressure drop correlations for two-phase flow within horizontal rectangular channels with small heights, International Journal of Multiphase Flow, 27 (2001) 783–796.

[10]. Benbella A. Shannak, Frictional pressure drop of gas liquid two-phase flow in pipes, Nuclear Engineering and Design. Nuclear Engineering and Design, 238(2008)3277–3284.

[11]. Ing Youn Chen, Yi-Min Chen et al, Two-phase frictional pressure drop in small rectangular channels, Experimental thermal and fluid science, 32(2007) 60-66.

[12]. G. Tryggvason, A. Esmaeeli, N. Al-Rawahi, Direct numerical simulations of flows with phase change, J. Computer. Structure, 83(2005) 445–453.

[13]. Erfeng Chen, Yanzhong Li, Xianghua Cheng, Lei Wang, Modeling of low-pressure subcooled boiling flow of water via the homogeneous MUSIG approach, Nuclear Engineering and Design, 239(2009)1733-1743.

[14]. Yang, Z., Peng, X.F., Ye, P. Numerical and experimental investigation of two phase flow during boiling in a coiled tube, J. International Journal of Heat and Mass Transfer, 51(2008) 1003–1016.

[15]. M.H. Yuan, Y.H. Yang, T.S. Li, Z.H. Hu, Numerical simulation of film boiling on a sphere with a volume of fluid interface tracking method, International Journal of Heat and Mass Transfer, 51 (2007) 1646-1657.

[16]. Mazumder, Quamrul H. CFD Analysis of Single and Multiphase Flow Characteristics in Elbow, J. Engineering, 4(2012) 210-221.

[17]. A. Giannoulis, Dimitrios-Periklis; Margaris, Dionissios P., Computational Study of the Two-Phase Oil-Water Flow Formed within the Vertical Pipe of a System Designed to Remove Leaking Oil from Maritime Accidents, J. International Review of Mechanical Engineering, 6(2012) 1694-1710.

[18]. Saffari, H.; Moosavi, R, Numerical study of the influence of geometrical characteristics of a vertical helical coil on a bubbly flow, J. Journal of Applied Mechanics & Technical Physics,55(2014) 957-965.

[19]. Harikrishnan G, et al, CFD Simulation of Subcooled Flow Boiling using OpenFOAM, International Journal of Current Engineering and Technology, 2(2014)441-447.

[20]. S.D.Changani et al, Engineering and Chemical Factors Associated with Fouling and Cleaning in Milk Processing, Experimental Thermal and Fluid Science,14(1997)392-406.

[21]. Youcef Mahdi et al, A dynamic model for milk fouling in a plate heat exchanger, Applied Mathematical Modeling, 33(2009) 648–662.

[22]. Helena E. C. Rummens, J. T. Rogers, C. W. Turner, The Thermal Hydraulics of Tube Support Fouling in Nuclear Steam Generators, Nuclear Technology,148(2004) 268-286.

[23]. Oleinik, s. G., Influence of various factors on damage to steam-generator tubes in nuclear power plants with VVÉR reactors, Atomic Energy, 96(2004) 399-402.

[24]. Thomas Pogiatzis, Edward M. Ishiyama,et al, Identifying optimal cleaning cycles for heat exchangers subject to fouling and ageing,applied energy,89(2012)60-66.

[25]. S. Sanaye, B. Niroomand, Simulation of heat exchanger network (HEN) and planning the optimum cleaning schedule, Energy Conservation Management,48(2007)1450–1461.

[26]. S. Jun, V. Puri, A 2D dynamic model for fouling of plate heat exchangers, Journal of Food Engineering, 75(2006)364–374.

[27]. Mariusz Markowski, Marian Trafczynski, Krzysztof Urbaniec, Validation of the method for determination of the thermal resistance of fouling in shell and tube heat exchangers, ・ Energy Conversion and Management, 76(2013) 307-313.

[28]. M. Abd-Elhady et al., Minimum gas speed in heat exchanger to avoid particulate fouling, International Journal of Heat and Mass Transfer, 47(2004)3843–3955.

[29]. M. Markowski, K. Urbaniec, Optimal cleaning schedule for heat exchangers in a heat exchanger network, Applied Thermal Engineering,25(2005)1019–1032.

[30]. Mostafa M. Awad, I. F. Abd El-Wahab and H. E. Gad, Effect of Surface Temperature on the Fouling of Heat Transfer Surfaces, Eleventh International Water Technology Conference, IWTC11 2007 Sharm El-Sheikh, Egypt, 283-298.

[31]. Jader R, Leong W, Geoffrey F, Flow Boiling of Water in a Vertical Tube at Sub-Atmospheric Pressures, Journal of the Brazilian Society of Mechanical Sciences and Engineering, 4(2007)401-409.

[32]. Yunlong Zhou et al. Experimental study on Onset of Nucleate Boiling in Rod Bundle Channel, Atomic Energy Science and Technology, 48(2014)1416-1420.

[33]. E. Krepper and R. Rzehak, CFD for subcooled flow boiling: simulation of DEBORA experiments, Nuclear Engineering and Design, 241(2011) 3851–3866.

[34].

[35].

[36].

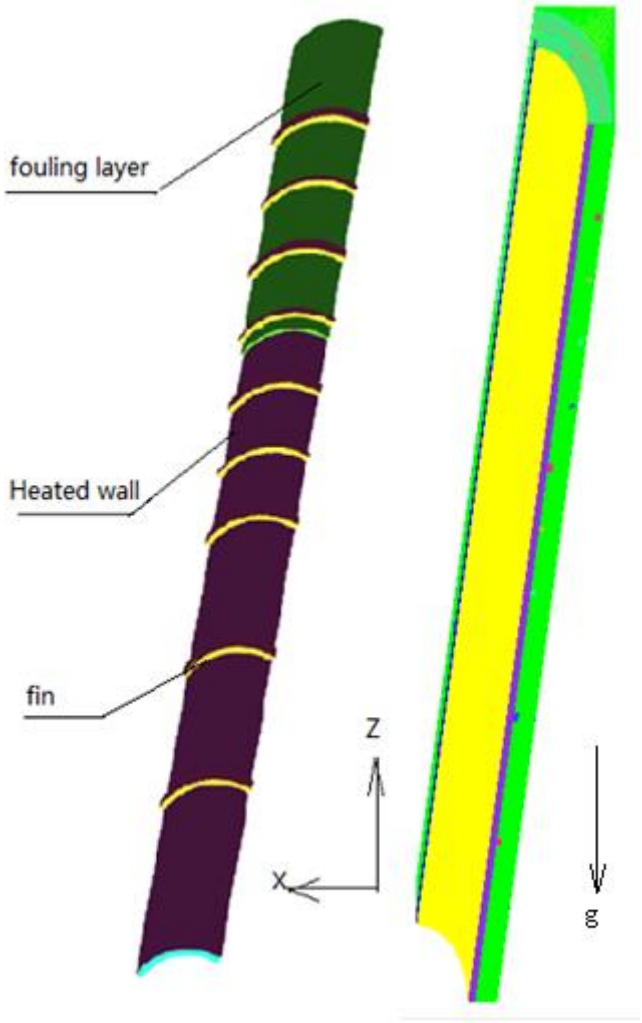

Figure 1 Sketch of the model

[37].

[38].

[39].

[40].

[41].

[42].

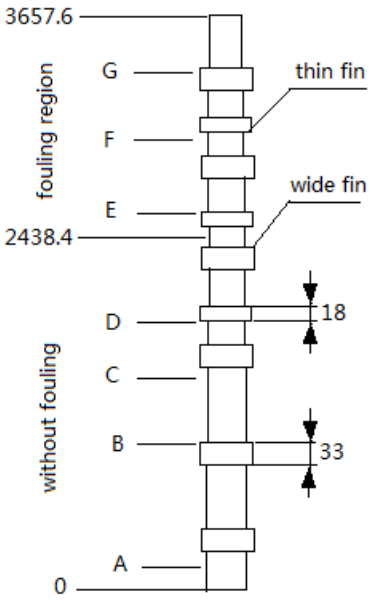

[43]

[4

Figure 2. Sketch of fins
All dimensions are in mm

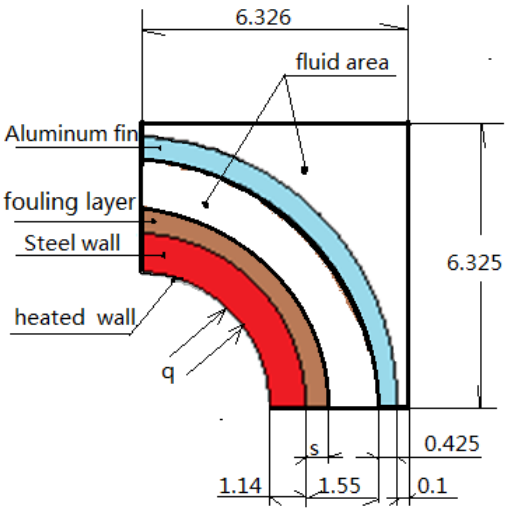

Figure 3. Cross section of the model

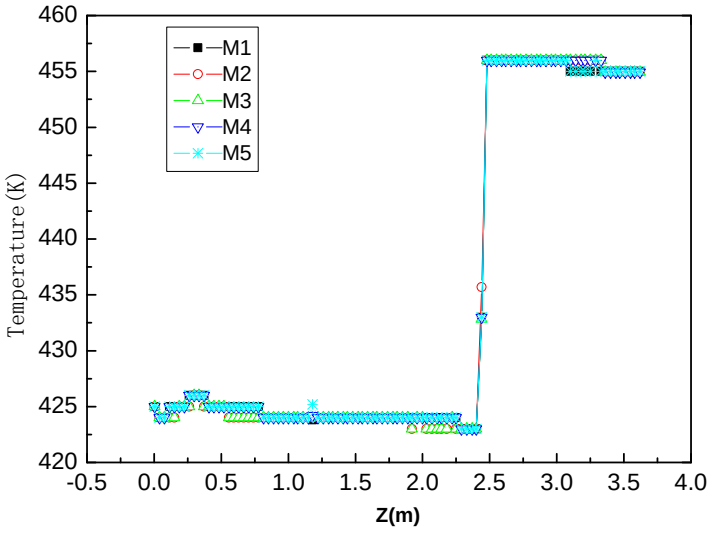

[45].

Figure 4. Bulk temperature profile at outer side of tube for each

[46].

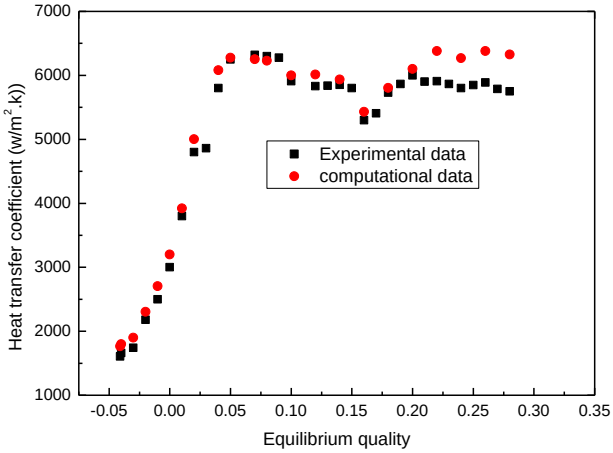

[47].

[48]. Figure 5. Comparison of computational results and measured data [31]

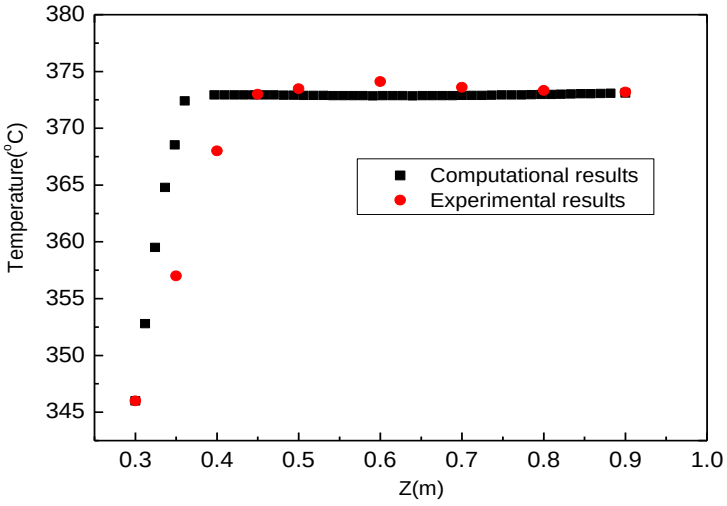

[49].

Figure 6. Comparison of numerical and experimental results [32]

[50].

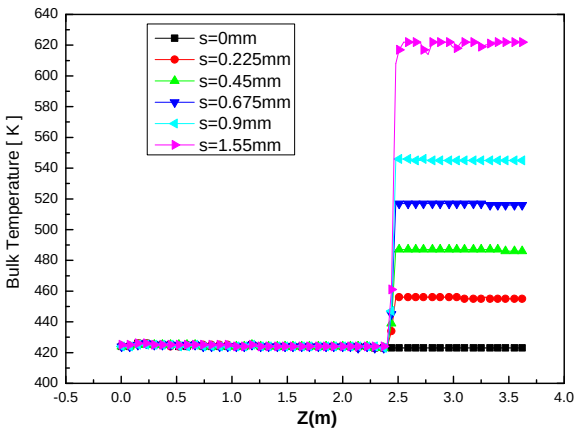

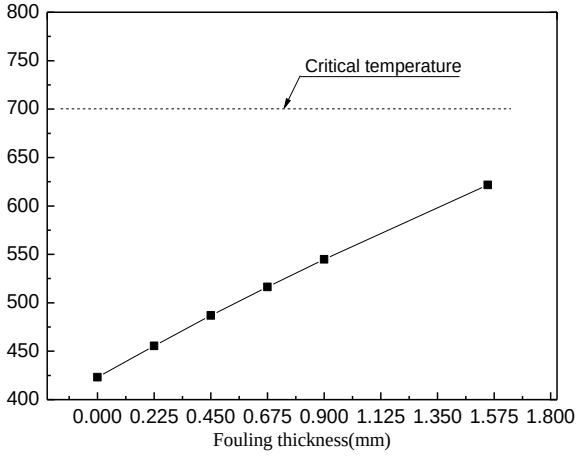

[51].

(a) along the channel (b) in the fouling region

Figure 7. Effect of different fouling thickness on bulk temperature

[52].

[53].

[54].

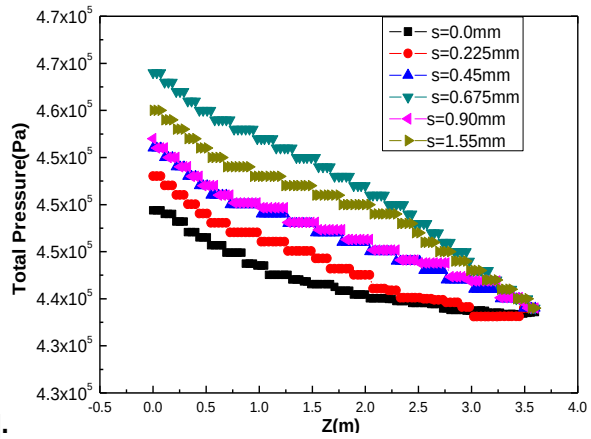

[55].

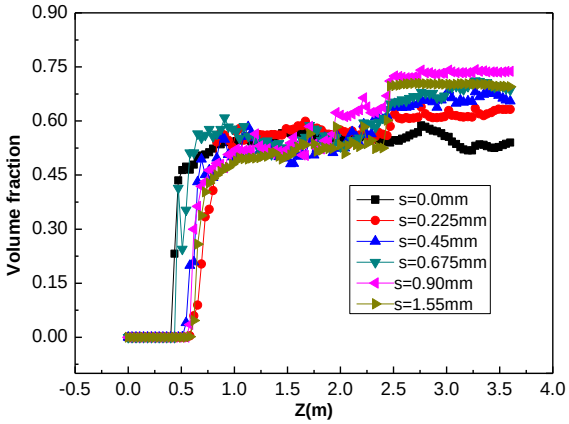

Figure 8. Distributions of total pressure along the channel

[56].

Figure 9. Distributions of vapor volume fraction along the channel

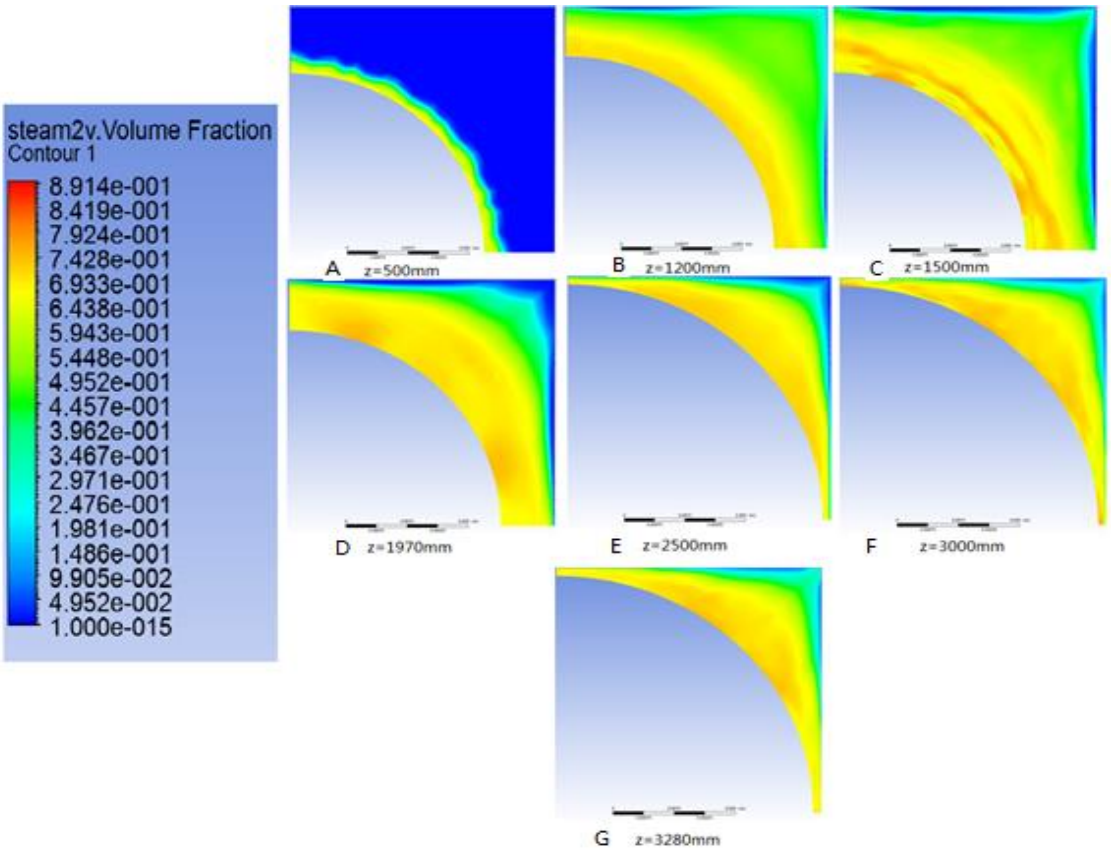

[57].

[58]. Figure 10. Contours representation of vapor volume fraction along the channel(s=1.55mm)

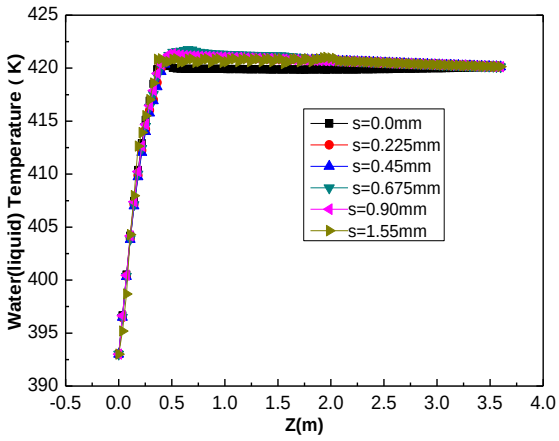

[59].

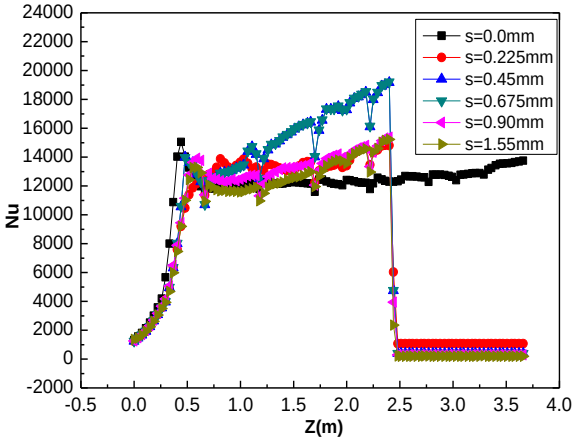

Figure11. Distributions of water (liquid) temperature along the channel **[60].**

Figure 12a . Effect of fouling thickness on the Nusselt number

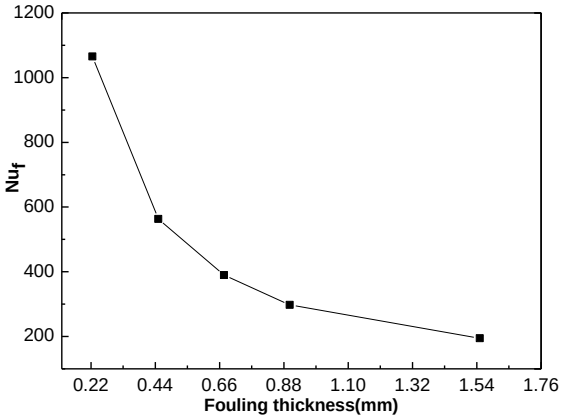

[61].

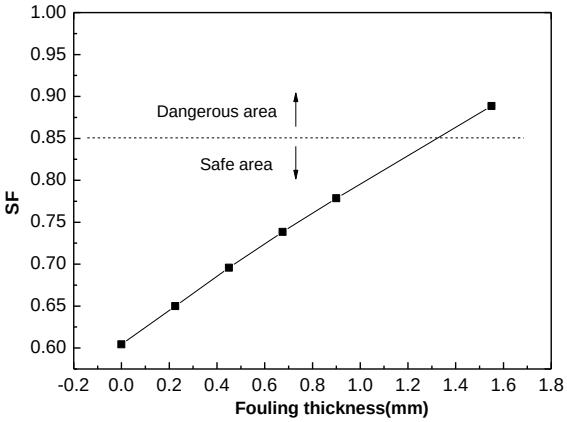

Figure 12b . Effect of fouling thickness on the Nusselt number(in fouling region)

[62].

Figure 12c . Effect of fouling thickness on security factor (in fouling region)

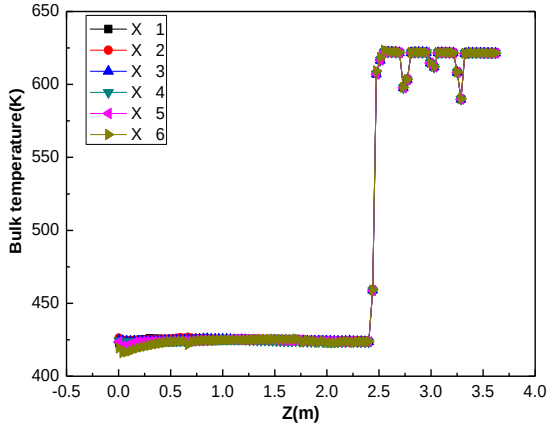

[63].

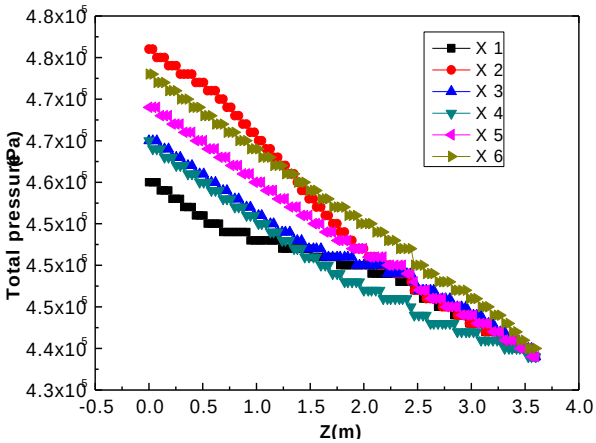

Figure13. Distributions of bulk temperature along the channel with different

[64].

Figure14. Distributions of pressure along the channel with different inlet velocities

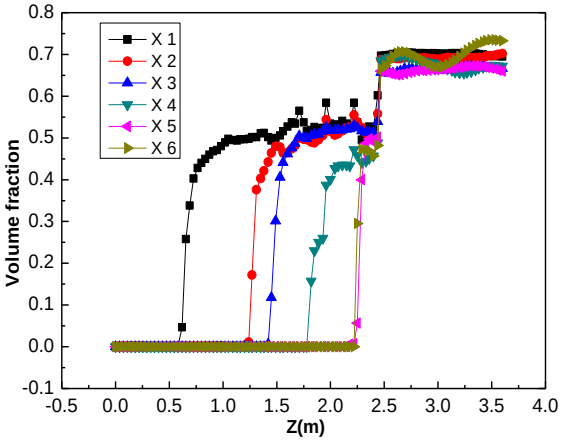

[65].

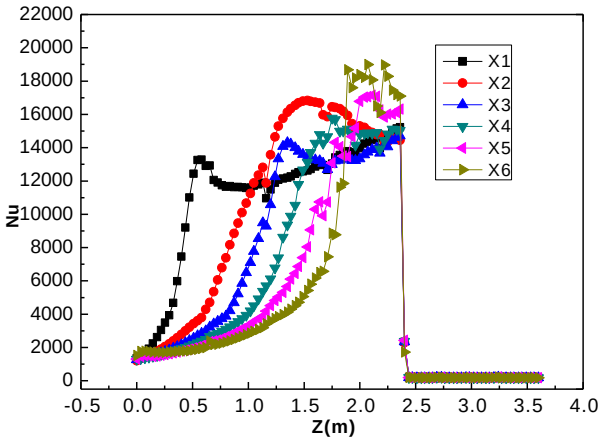

Table 1 Detailed structure of the model

	Region name	*(Z) From (mm)*	*(Z) To(mm)*	*Total Height (mm)*
Without fouling laye	*Heated Wall(HW) first part*	*0*	*647.7*	*647.7*
	First wide fin	*647.7*	*680.7*	*33*
	HW.Second part	*680.7*	*1169.7*	*489*
	Second wide fin	*1169.7*	*1202.7*	*33*
	HW.Third part	*1202.7*	*1691.7*	*489*
	Third wide fin	*1691.7*	*1724.7*	*33*
	HW. Fourth part	*1724.7*	*1960.2*	*235.5*
	First thin fin	*1960.2*	*1978.2*	*18*
	HW. Fifth part	*1978.2*	*2213.7*	*235.5*
	Fourth wide fin	*2213.7*	*2246.7*	*33*
	HW.Sixth part(1)	*2246.7*	*2438.4*	*191.7*
	HW.Sixth part(1)	*2438.4*	*2482.2*	*43.8*

	Second thin fin	*2482.2*	*2500.2*	*18*
	HW. Seventh part	*2500.2*	*2735.6*	*235.4*
	Fifth wide fin	*2735.6*	*2768.6*	*33*
	HW. Eighth part	*2768.6*	*3004.1*	*235.5*
	Third thin fin	*3004.1*	*3022.1*	*18*
	HW. Ninth part	*3022.1*	*3257.6*	*235.5*
	Sixth wide fin	*3257.6*	*3290.6*	*33*
	HW.Tenth part	*3290.6*	*3657.6*	*367*

Table 2. Designations and number of cells

Mesh designation	*Number of cells in domain*
M1	*722350*
M2	*819500*
M3	*1123100*
M4	*1232000*
M5	*1623200*